



SIMULATION OF A DIRECT REDUCTION MOVING BED REACTOR USING A THREE INTERFACE MODEL

A. Mirzajani¹, H. Ale Ebrahim¹ and S.M.M. Nouri^{2,*}

¹ Chemical Engineering Department, Petrochemical Center of Excellence,
AmirKabir University of Technology, Tehran 15875-4413, Iran

² Chemical Engineering Department, Hakim Sabzevari University, Sabzevar, Iran

(Submitted: April 2, 2017; Revised: July 17, 2017; Accepted: August 30, 2017)

Abstract - In the present study, the rate of reduction in the direct reduction moving bed reactor of a MIDREX plant has been studied. The reactor was modeled by a one-dimensional, nonisothermal, steady-state model. The three interface unreacted shrinking core model accounting for different iron oxides reduction was used for describing the reaction behaviors at the pellet scale. The quasi steady state assumption was used to calculate the gas species concentrations at the interfaces. The effects of external and internal mass transfer resistance through the pellets and heat transfer on the overall rate of reduction were considered. The results of the model were validated with the data of the Khorasan Steel plant (Neyshabur, Iran). The model results show good agreement with the plant data. The effect of gas and solid flow rates, feed gas properties, and pellet characteristics on the reactor performance were investigated using the model.

Keywords: Simulation, Direct reduction, Moving-bed reactor, Unreacted shrinking core model, Three interface model.

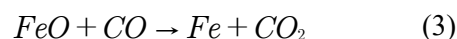
INTRODUCTION

Direct reduction of hematite with synthesis gas as the reducing agent is a well-established process for the production of solid iron with considerably low greenhouse emission (Kim and Worrell, 2002). The world direct reduced iron (DRI) production has increased from 790 kt/yr in 1970 to 74.55 Mt/yr in 2014. Iran is the second largest producer of sponge iron in the world (14.55 Mt/yr), mostly using the MIDREX process for iron production (Pineau et al., 2006) (MIDREX, 2014).

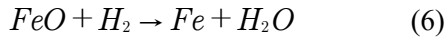
The direct reduction reactor is a moving-bed reactor in which pellets are loaded at the top of the bed and move countercurrent to the reducing gas,

which is injected at the bottom. The sponge iron is removed as product at the bottom.

The iron oxide is reduced to sponge iron via the following reactions:



*Corresponding author. E-mail address: m.nouri@hsu.ac.ir



Direct reduction has been investigated for three decades and different mathematical models were introduced in order to predict the reaction behavior. Direct reduction is a complex phenomenon in which many parameters have influence on the reaction behavior. It is neither possible nor necessary to consider all the parameters in the mathematical model. So, all the models developed up to now have used some simplifying assumptions and neglected the parameters which have less importance in the reduction reactor.

Almost all of the models developed for the direct reduction reaction neglected the accumulation term and assumed that the reaction is pseudo steady state (Beheshti et al., 2014; Negri et al., 1991; Nouri et al., 2011; Parisi and Laborde, 2004; J Szekely and El-Tawil, 1976; Tsay et al., 1976; Mohammad Sadegh Valipour and Saboohi, 2007). Among the mathematical models applied to the iron ore reduction, the shrinking core model has been used in most of the works, which assumes that there is a sharp interface between the reacted and unreacted zones (Beheshti et al., 2014; Negri et al., 1991; Parisi and Laborde, 2004). Also, most of the researches to date tended to focus on the pellet scale and pilot scale modeling rather than an industrial reactor (Nouri et al., 2011; Parisi and Laborde, 2004). Moreover, research on the subject has been mostly restricted to the pure reducing gases as the reducing agents (H_2 or CO or a mixture of H_2 and CO) and the effect of real gas conditions were neglected (Hou et al., 2015; Jozwiak et al., 2007; Monazam et al., 2014; Negri et al., 1991; M. S. Valipour et al., 2006). Considering global reduction reaction rates (hematite to metallic iron) is another simplifying assumption used by some researchers (Nouri et al., 2011; Parisi and Laborde, 2004). This actually assumes that the reduction of hematite to iron has just one controlling step and the kinetic constant of this step was used for the overall reaction. Other researchers also neglected some controlling steps such as external mass transfer of gas reactants to the pellet surface (Beheshti et al., 2014), diffusion of gas reactant through the pores inside the pellet and the iron oxides to the reaction surface (Hou et al., 2015).

In this work, the industrial direct reduction reactor of the Khorasan Steel plant was modeled using a mathematically simple but accurate model. Also the effects of operating parameters such as gas and solid

flow rates, H_2/CO ratio, reducing gas potential, and pellet size on the reactor performance have been studied.

MATHEMATICAL MODELING

Pellet scale

A three interface model (hematite/magnetite, magnetite/wustite, and wustite/iron) based on the unreacted shrinking core model has been developed for the prediction of pellet behavior in the direct reduction reactor. The model assumptions are as follow:

- 1) The hematite pellets are non-porous.
- 2) The reactions are reversible.
- 3) The pellets reacted at three sharp interfaces (hematite/magnetite, magnetite/wustite, and wustite/iron) with reducing gases.
- 4) The pellet diameter remains constant during the reaction.
- 5) The side reactions between the gaseous species are neglected.

The reaction rates of different iron oxides with reducing gases at each interface determine how the radius of the interfaces changes during the reduction.

The key step in the use of the three-interface unreacted shrinking core model is the calculation of reducing gases concentrations (H_2 and CO) and also the produced gases concentrations (H_2O and CO_2) at each interface using the quasi steady state assumption as follows (Bischoff, 1963; Q. T. Tsay et al., 1976):

$$C_A^{w-Fe} = C_A^b - \left[\frac{R_{F,A} + R_{S,A}^{Fe}}{\Omega_C [R_{F,A} + R_{S,A}^{Fe}] + \frac{\Omega_D [R_{F,A} + R_{S,A}^{Fe}]}{k_e^{w-Fe} k_e^{m-w} k_e^{h-m}} + 1} \right] \quad (7)$$

$$\left[\Omega_C C_A^b - \frac{\Omega_D}{k_e^{w-Fe} k_e^{m-w} k_e^{h-m}} C_B^b \right]$$

$$C_A^{m-w} = C_A^{w-Fe} - \left[\frac{R_{S,A}^w}{\Omega_d R_{S,A}^w + \frac{\Omega_b R_{S,B}^w}{k_e^{m-w} k_e^{h-m}} + 1} \right] \quad (8)$$

$$\left[\Omega_d C_A^{w-Fe} - \frac{\Omega_b C_B^{w-Fe}}{k_e^{m-w} k_e^{h-m}} \right]$$

$$C_A^{h-m} = C_A^{m-w} - \left[\frac{R_{S,A}^m}{R_{S,A}^m + R_j^{h-m} + \frac{R_{S,B}^m}{k_e^{h-m}}} \right] \left[C_A^{m-w} - \frac{C_B^{m-w}}{k_e^{h-m}} \right] \quad (9)$$

Equations for calculation of Ω_1 can be found elsewhere (Q. T. Tsay et al., 1976). Equations (7) and (8) show the concentrations of hydrogen and carbon

monoxide at the wustite/iron interface and magnetite/wustite interface, respectively. Also equation (9) shows the concentration of these gaseous species at the hematite/magnetite interface (concentration at the unreacted core). The following superscripts represent the various iron oxides: hematite/magnetite (h-m), magnetite/wustite (m-w), and wustite /iron (w-Fe). Equations (10)-(12) show the concentration of product gases (Q. T. Tsay et al., 1976).

$$C_B^{w-Fe} = C_B^h + \left[\frac{R_{F,B} + R_{S,B}^{Fe}}{R_{F,A} + R_{S,A}^{Fe}} \right] \cdot [C_A^h - C_A^{w-Fe}] \quad (10)$$

$$C_B^{m-w} = C_B^{w-Fe} + \left[\frac{R_{S,B}^w}{R_{S,A}^w} \right] \cdot [C_A^{w-Fe} - C_A^{m-w}] \quad (11)$$

$$C_B^{h-m} = C_B^{m-w} + \left[\frac{R_{S,B}^m}{R_{S,A}^m} \right] \cdot [C_A^{m-w} - C_A^{h-m}] \quad (12)$$

The diffusion of hydrogen and carbon monoxide into the pellets is affected by several resistances from the bulk gas to each reaction interface.

The mass transfer resistance for all gaseous species from the bulk gas to the outer surface of the pellets is expressed by equation (13). The diffusion resistance between the porous iron surface and the iron/wustite interface is presented in equation (14). The diffusion resistance between the wustite/magnetite and magnetite/hematite interfaces can be stated by equations (15) and (16) respectively. Also the reaction resistances at each interface are presented in equation (17).

$$R_{f,j} = \frac{R_g T_s}{k_{m,j} 4\pi r_p^2} \quad j = A,B \quad (13)$$

$$R_{s,j}^{Fe} = \frac{R_g T_s}{D_{eff,j}^{Fe}} \cdot \frac{r_p - r^{w-Fe}}{4\pi r^{w-Fe} r_p} \quad (14)$$

$$R_{s,j}^w = \frac{R_g T_s}{D_{eff,j}^w} \cdot \frac{r^{w-Fe} - r^{m-w}}{4\pi r^{m-w} r^{w-Fe}} \quad (15)$$

$$R_{s,j}^m = \frac{R_g T_s}{D_{eff,j}^m} \cdot \frac{r^{m-w} - r^{h-m}}{4\pi r^{h-m} r^{m-w}} \quad (16)$$

$$R_{j,i}^{t-s} = \frac{R_g T_s}{k_{r,i}^{t-s} 4\pi (r^{t-s})^2} \quad (17)$$

Reactor scale modeling

The reactor investigated in this study is a typical direct reactor of a MIDREX plant. The iron oxide pellets are loaded at the top of the reactor and move downward. The reduction process is accomplished

by the upward reducing gases through the iron oxide pellets by reactions (1)-(6).

The following assumptions have been considered for derivation of the mass and energy balance equations:

- 1) The gas and solid phases are in plug flow and also axial and radial dispersions are negligible.
- 2) The gas flow is uniform radially.
- 3) Gas mixture is ideal.
- 4) The reduction reactor is at steady state condition.
- 5) All the reactions are first order and reversible.

Considering these assumptions, the mass balance equations for the gas phase are expressed by equations (18) and (19). These equations represent variations of reducing gas concentration along the reactor.

$$\frac{dC_{CO}}{dz} = -\frac{C_t}{G} [\phi^{h-m} R_{CO}^{h-m} + \phi^{m-w} R_{CO}^{m-w} + \phi^{w-Fe} R_{CO}^{w-Fe}] \quad (18)$$

$$\frac{dC_{H_2}}{dz} = -\frac{C_t}{G} [\phi^{h-m} R_{H_2}^{h-m} + \phi^{m-w} R_{H_2}^{m-w} + \phi^{w-Fe} R_{H_2}^{w-Fe}] \quad (19)$$

Equation (20) describes the interface position of the pellets at any point of the reactor (Tsay et al., 1976).

$$\frac{dr^{t-s}}{dz} = -\frac{1}{\rho_r \phi^{t-s} (1 - \varepsilon_t) u_s} \cdot \left[K_{r,CO}^{t-s} \left(C_{CO}^{t-s} - \frac{C_{CO}^{t-s}}{k_{e,CO}^{t-s}} \right) + K_{r,H_2}^{t-s} \left(C_{H_2}^{t-s} - \frac{C_{H_2}^{t-s}}{k_{e,H_2}^{t-s}} \right) \right] \quad (20)$$

The reaction rate at each interface of the pellet is the sum of both reducing gas reaction rates with various iron oxides at the interface.

Energy balance for the gas and solid phases can be written as follows (Nouri et al., 2011):

$$\frac{dT_g}{dz} = \frac{h_c a_s}{-GC_{ps}} \cdot [T_g - T_s] \quad (21)$$

$$\frac{dT_s}{dz} = \frac{h_c a_s}{(1 - \varepsilon_b) \cdot u_s \cdot \rho C_{ps}} (T_g - T_s) + \frac{1}{(1 - \varepsilon_b) \cdot u_s \cdot \rho C_{ps}} \sum_{i=CO,H_2} \sum_{t-s} \Delta H_i^{t-s} R_i^{t-s} \quad (22)$$

The physical properties of the solid phase such as porosity, heat capacity and density change from the top to the bottom of the reactor. Therefore, these properties should be calculated along the reactor.

The volumetric heat capacity of the pellets presented in equation (23) is a function of physical and chemical properties of each solid layer (hematite, magnetite, wustite, and iron) (Tsay et al., 1976).

$$\overline{\rho_s C_{ps}} = \rho_h C_{ph} (1 - \varepsilon_h) \left[\frac{r^{h-m}}{r_p} \right]^3 + \rho_m C_{pm} (1 - \varepsilon_m) \left[\frac{(r^{m-w})^3 - (r^{h-m})^3}{r_p^3} \right] + \rho_w C_{pw} (1 - \varepsilon_w) \left[\frac{(r^{w-Fe})^3 - (r^{m-w})^3}{r_p^3} \right] + \rho_{Fe} C_{pFe} (1 - \varepsilon_{Fe}) \left[1 - \frac{(r^{w-Fe})^3}{r_p^3} \right] \quad (23)$$

Reaction rate equation

In the three interface model, the reduction rates of iron oxides in the different reaction steps (hematite to magnetite, magnetite to wustite, and wustite to iron) can be calculated as follows (Tsay et al., 1976):

$$R_A^{t-s} = \frac{3(1-\epsilon_b)}{r_p^3} \cdot (r^{t-s})^2 \phi^{t-s} K_r^{t-s} \left(C_A^{t-s} - \frac{C_B^{t-s}}{K_{e,A}^{t-s}} \right) \quad (24)$$

Subscript A indicates the reducing gases hydrogen and carbon monoxide and $t-s$ is related to different interfaces within the pellets.

Boundary conditions for the mass and energy balances along the reactor are as follows:

At the solid inlet (top):

$$r^{h-m}(z=0) = r_p \quad (25)$$

$$r^{m-w}(z=0) = r_p \quad (26)$$

$$r^{w-Fe}(z=0) = r_p \quad (27)$$

$$T_s(z=0) = T_{s0} \quad (28)$$

At the gas inlet (bottom):

$$C_{H_2}(z=L) = C_{H_2}^0 \quad (29)$$

$$C_{CO}(z=L) = C_{CO}^0 \quad (30)$$

$$T_g(z=L) = T_g^0 \quad (31)$$

Combination of the pellet and reactor scale equations leads to seven ordinary differential equations. The Runge-Kutta method was used to solve the mass and energy balance equations and the boundary value problem was reduced to an initial value problem using the shooting method (Dormand and Prince, 1980). In the shooting method, we first guessed three missing boundary conditions at the top of the reactor and solved the differential equations with these initial boundary conditions using the Runge-Kutta method. Then the resulting boundary conditions at the bottom of the reactor were compared with actual fixed values (temperature and concentration of gas phase) and, by changing the assumed initial boundary conditions,

repeated the above steps again until these values were approximately equal within a given tolerance.

Parameter calculation

Porosity

The intermediate solid products (magnetite, wustite, and iron) are porous; therefore, assuming no volume change of pellets along the reactor, the following equations were used to calculate the porosity of solids (Tsay et al., 1976):

$$\epsilon_{Fe} = 1 - (1 - \epsilon_h) \frac{2\rho_h}{\rho_{Fe}} \quad (32)$$

$$\epsilon_w = 1 - (1 - \epsilon_h) \frac{2\rho_h}{\rho_w} \quad (33)$$

$$\epsilon_m = 1 - (1 - \epsilon_h) \frac{2\rho_h}{3\rho_m} \quad (34)$$

The porosity of different oxides and metallic iron can be seen in Table 2.

Diffusion coefficients

The effective diffusivity of gas reactants through the solid pores can be obtained as follows:

$$\frac{1}{D_{e0}} = \frac{1}{\epsilon_0^2} \left(\frac{1}{D_{AM}} + \frac{1}{D_{AK}} \right) \quad (35)$$

where D_{AM} is the molecular diffusivity, which was estimated from the Slattery and Bird equation (Bird et al., 2007) and D_{AK} is the Knudsen diffusivity, calculated as (J. Szekely et al., 1976):

$$D_{AK} = 9700 \times \frac{2\epsilon_0}{S_0} \left(\frac{T}{M_w} \right)^{0.5} \quad (36)$$

Heat and mass transfer coefficients

The following empirical equation was used for calculation of the heat transfer coefficient between the gas and the solid pellets in a moving bed reactor (Akiyama et al., 1993):

$$Nu = 2 + 0.39 Re_p^{1/2} Pr^{1/3} \quad (37)$$

The mass transfer coefficient was obtained using the analogy between heat and mass transfer.

$$Sh = 2 + 0.39 Re_p^{1/2} Sc_j^{1/3} \quad (38)$$

Activation energy, rate constant and equilibrium constant

The kinetic data proposed by (Takenaka et al., 1986) was used in this work. The Arrhenius relation is used in order to calculate the rate constants for the reduction reactions. Frequency factors, activation energies and equilibrium constants for the reactions are listed in Table 1.

RESULTS AND DISCUSSION

In this section, the model developed was validated using reduction reactor data of the Foolad Khorasan plant (Neyshabur, Iran). Then, the model was used to predict the reactor behavior for different operational conditions. The operational conditions of the industrial plant are shown in Table 2.

A comparison between the results of the mathematical model and the plant data are listed in Table 3. As can be seen, deviations of the model results from the plant data are negligible.

Figure 1 presents the variation of gas and solid temperatures along the reactor. It is obvious that the both solid and gas temperatures increase from the top to the bottom of the reactor. Due to the heat that the reduction reactions release and absorb on the surface of iron oxides pellets, the temperatures of the solid and gas phases are equal in the bottom of the reactor. Since most of the endothermic reactions happen in the top half of the reactor, the decrease of the gas temperature is considerable in this section. The bold points are the boundary temperatures of the reactor (at the top and bottom of the reactor).

The variations of gas composition along the reactor can be seen in Figure 2. The reducing gas contains hydrogen, carbon monoxide, water vapor, carbon dioxide and inert gases. As the reaction proceeds and the reducing gases move upward in the reactor, the concentrations of hydrogen and carbon monoxide decrease and the concentrations of product gases

Table 2. Operating conditions of the Khorasan plant.

Gas				
Gas flow rate	170000 Nm ³ /h			
H ₂	54.43			
CO	34.51			
H ₂ O	4.82			
CO ₂	3.38			
CH ₄ +N ₂	3.84			
Inlet temperature	1193 K			
Solid				
Production (Fe)	110 ton/h			
Mineral pellet density	4.1 g/cm ³			
Sponge iron density	3.1 g/cm ³			
Pellet radius(r0)	0.5 cm			
Porosity	H	M	W	Fe
	0.204	0.232	0.364	0.635
Reactor				
reaction zone length	1000 cm			
Diameter	560 cm			

(water vapor and carbon dioxide) increase. The bold points show the mole fractions of output gases at the top of the Khorasan plant.

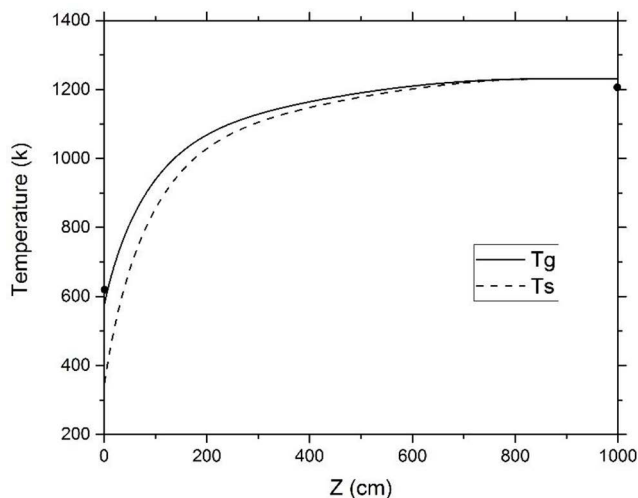
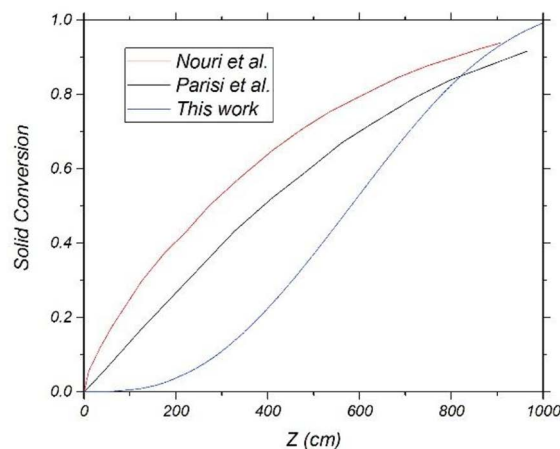
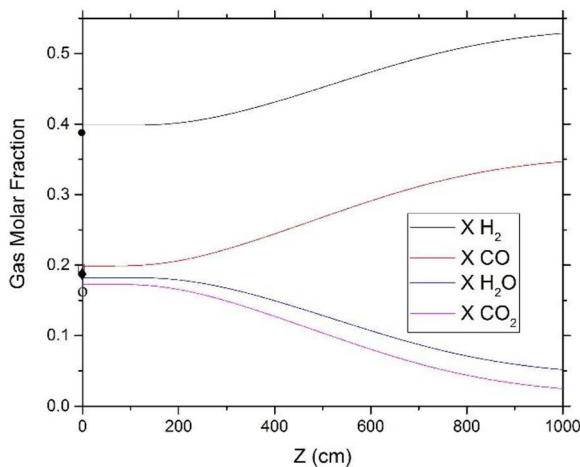
There is a difference between the solid conversion profiles developed by this model and some previous published works (Nouri et al., 2011; Parisi and Laborde, 2004). As can be seen in Figure 3, in the first two meters of the reactor, the solid conversion curve shows slight change and after that, it rises relatively fast to its final value. But for other models, the trends steadily rise for the first 6 meters of the reactor and the rates slow down gradually after that. This may be explained by the methods used by the different models for defining the conversion equation. In this work, the solid conversion was defined as the amount of wustite layers reduced to metallic iron and, since the hematite layers at the top of the reactor were reduced to magnetite first, the solid conversion in that area was near to zero. In the other models, only the overall direct reduction reactions were considered, resulting

Table 1. Frequency factors, activation energies and equilibrium constants of reactions (Takenaka et al., 1986).

Reactions	K ₀ (cm/s)	E _a (J/mol)	K _e = A exp(B/T)	
			A	B
$3Fe_2O_3 + H_2 \leftrightarrow 2Fe_3O_4 + H_2O$	16000	92092	30761	-362.6
$Fe_3O_4 + H_2 \leftrightarrow 3FeO + H_2O$	2300	71162	4722	-7916.6
$FeO + H_2 \leftrightarrow Fe + H_2O$	3000	63627	2.54	1586.9
$3Fe_2O_3 + CO \leftrightarrow 2Fe_3O_4 + CO_2$	270000	113859	51.42	968.37
$Fe_3O_4 + CO \leftrightarrow 3FeO + CO_2$	2500	73674	7942.64	-3585.6
$FeO + CO \leftrightarrow Fe + CO_2$	1700	69488	0.053	2744.6

Table 3. Comparison between the model results and plant data.

Outlet gas composition	Model data (dry base) (%)	Foolad Khorasan data (dry base) (%)
Hydrogen	48.73	45 ± 2
Carbon monoxide	24.3	23.8 ± 1
Carbon dioxide	21.2	23.1 ± 1.2
Nitrogen and Methane	5.77	5.7 ± 0.8
Solid conversion	94.14	93.7 ± 1
Gas outlet temperature	580 k	620 k

**Figure 1.** Temperature profiles of the gas and solid along the reactor calculated by the model (the dots on the temperature axis are the solid and gas input temperature).**Figure 3.** Comparison between the solid conversion profiles created in this work and other published works (Nouri et al., 2011; Parisi and Laborde, 2004).**Figure 2.** Composition profiles of gases along the reactor (points below and above H₂ •, H₂O ♦, CO □ and CO₂ ○; composition lines show the outlet gas composition of the reactor).

in the constant increase of solid conversion in the solid inlet section.

Effect of feed gas composition

Figure 4 shows the effect of feed gas composition on the solid conversion. The experimental results of

Taknaka confirmed that the overall rate of reduction decreases upon increasing the ratio of hydrogen to carbon monoxide (Takenaka et al., 1986). This result is likely to be related to the heat of reduction of H₂ and CO with iron oxides. The majority of the reduction reactions with hydrogen are endothermic. Therefore, with increasing hydrogen concentration, the portion of reduction reactions with hydrogen increases which result in a decrease in the reactor temperature and overall reduction rates. On the other hand, the majority of reduction reactions with carbon monoxide are exothermic, and the solid conversion rate increases with increasing carbon monoxide concentration in the feed gas due to the increase in the reactor temperature and consequently the rate of reduction reactions.

It should be noted that, if the concentration of carbon monoxide is greater than the hydrogen concentration in the feed gas, the possibility of coke deposition on the sponge iron increases, which leads to a decrease in the reduction rate due to increasing diffusional resistances. So, the H₂/CO ratio is usually greater than one.

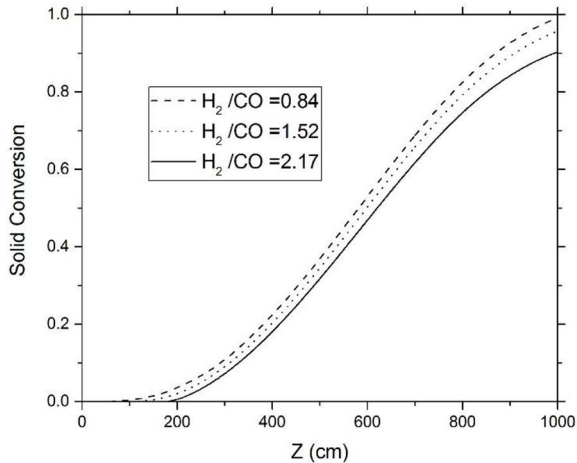


Figure 4. Effect of the reducing gases ratio on the solid conversion calculated by the model.

Effect of feed gas potential

The gas potential is defined as the ratio of hydrogen and carbon monoxide concentration to water vapor and carbon dioxide concentrations or $(H_2+CO)/(H_2O+CO_2)$. In the direct reduction processes, this parameter depends on the reformer operating conditions, that usually change within 5-49 (Takenaka et al., 1986). It can be seen in Figure 5 that the reduction decreases for lower gas potential due to the decrease in the reducing gas concentrations.

Effect of pellet size

Figure (6) shows the effect of pellet size on the solid conversion. As the pellet size decreases, the active surface exposed to the reducing gases increases. So, the

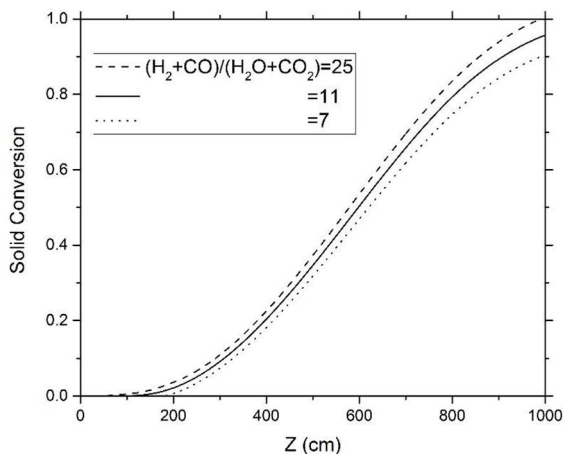


Figure 5. Effect of gas potential on the solid conversion calculated by the model.

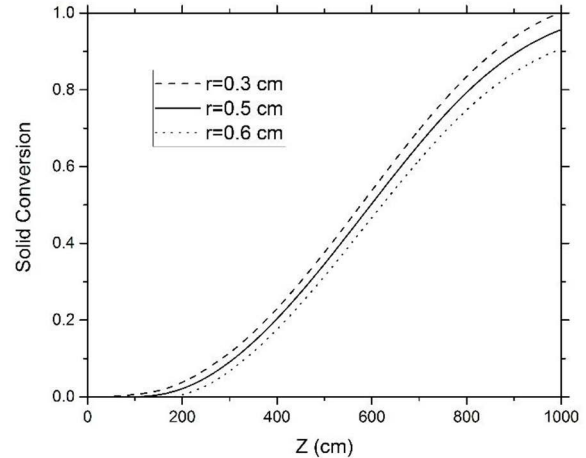


Figure 6. Effect of pellet size on the solid conversion calculated by the model.

diffusion path within the pellet decreases and the solid conversion increases respectively. It should be noted that, in this case, the gas phase pressure drop along the reactor will increase considerably. Previous researches show that the pressure drop is inversely proportional to the cubed value of the bed void fraction and void fraction increases with pellet size (Afandizadeh and Fourny, 2001; Brunner et al., 2015).

Effect of gas flow rate

The effect of gas flow rate on the solid conversion is presented in figure (7). As the gas flow rate is increased, the concentration of reducing gases and the gas velocity are increased. So, Reynolds number, heat and mass transfer coefficients are consequently increased according to equations (37) and (38). Increasing the mass transfer coefficient between the bulk gas and the pellet surface results in an increase in the concentration of reducing gases on the pellet surface, which decreases the effect of mass transfer on the overall rate of reaction. Also with increasing heat transfer coefficient, the solid temperature rises, leading to an increase in the reaction rate and solid conversion.

CONCLUSIONS

The purpose of the current study was to investigate the behavior of an industrial direct reduction reactor using a relatively simple mathematical model. A model based on the three interface unreacted shrinking core model at the pellet scale, combined with mass and energy balances for the reactor, has been developed in this work.

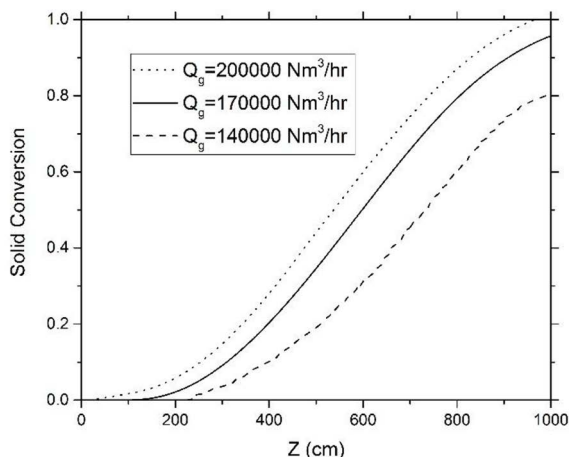


Figure 7. Effect of gas flow rate on the conversion of iron ore calculated by the model.

The results of this study confirm that the direct reduction reactor behavior can be predicted with considerably high precision using the model.

This study has shown that the pellet size and gas flow rate exert the most important effects on the conversion of iron oxide. A limitation of this study is that most of the industrial data are available only for the top and bottom of the reactor and not along the reactor. So, the validity of the model could not be compared throughout the reactor.

ACKNOWLEDGMENT

We would like to show our gratitude to the Foolad Khorasan Company for the contribution of the plant data.

NOMENCLATURE

A	related to hydrogen and carbon monoxide (mol/cm ³)
a _s	total pellet surface area per unit bed volume (cm ² /cm ³)
B	related to water vapor and carbon dioxide (mol/cm ³)
C _t	total concentration of inlet gas (mol/cm ³)
C _A ^{t-s}	concentration of gas component A at the interface t-s (mol/cm ³)
C _B ^{t-s}	concentration of gas component B at the interface t-s (mol/cm ³)
C _p	heat capacity (J/mol.k)
C _i ^{h-m}	concentration of gas component i at the interface h-m (mol/cm ³)
C _i ^{m-w}	concentration of gas component i at the interface m-w (mol/cm ³)
C _i ^{w-f}	concentration of gas component i at the interface w-f (mol/cm ³)

C _i ^B	concentration of gas component i in bulk phase (mol/cm ³)
D _{eff}	effective diffusivity (cm ² /s)
D _{ij}	binary diffusivity (cm ² /s)
D _{i,m}	diffusivity of component i in multi component system (cm ² /s)
E	activation energy (J/mol)
G	molar flow of gas phase (mol/cm ² s)
h _c	heat transfer coefficient (W/K.cm ²)
K _{r,A} ^{t-s}	specific rate constant for reaction from t to s species (cm/s)
K _e ^{t-s}	equilibrium constant for reaction from t to s species
k _m	heat transfer coefficient (cm/s)
M _w	Molecular weight (g/mol)
Nu, Re	Nusselt and Reynolds numbers, respectively
Sc, Sh	Schmidt and Sherwood numbers, respectively
r ^{t-s}	radius of interface between t and s species (cm)
R _A ^{t-s}	reaction rate from t to s per unit volume of bed (mol/cm ³ s)
R _g	gas constant
r _p	pellet radius (cm)
T _s , T _g	solid and gas phase temperatures (K)
t-s	related to various interfaces h-m, m-w, w-Fe
u _s , u _g	gas and solid velocity (cm/s)
Z	distance from the top of the bed (cm)

Greek letters

ρ _t	true molar density of t species (mol/cm ³)
ρ _{rs} , ρ _{ps}	true molar density of reactant and product solids (mol/cm ³)
τ	tortuosity factor
φ ^{t-s}	oxygen density change from t to s species, φ ^{h-m} =0.333, φ ^{m-w} =0.832, φ ^{w-Fe} =1 (atm O/mol t)
ε _b	void fraction of the bed
ε _t	void fraction of t phase
ΔH	heat of reaction (J/mol)

Subscripts

h	hematite
m	magnetite
w	wustite
Fe	iron

REFERENCES

- Afandizadeh, S., and Foumeny, E. A. Design of packed bed reactors: guides to catalyst shape, size, and loading selection, *Appl. Therm. Eng.*, 21, No 6), 669-682 (2001).

- Akiyama, Tomohiro, Takahashi, Reijiro, and Yagi, Jun-ichiro.. Measurements of heat transfer coefficients between gas and particles for a single sphere and for moving beds, *ISIJ. Int.*, 33, No 6), 703-710 (1993).
- Beheshti, Reza, Moosberg-Bustnes, John, and Aune, Ragnhild E. Modeling and simulation of isothermal reduction of a single hematite pellet in gas mixtures of H₂ and CO. Paper presented at the 143rd Annual Meeting and Exhibition, TMS 2014, San Diego, CA; United States (2014)
- Bird, R.B., Stewart, W.E., and Lightfoot, E.N. *Transport phenomena* (Revised 2 ed.). Wiley, New York (2007)
- Bischoff, K. B. Accuracy of the pseudo steady state approximation for moving boundary diffusion problems, *Chem. Eng. Sci.*, 18, No 11), 711-713 (1963).
- Brunner, Kyle M., Perez, Hector D., Peguin, Robson P. S., Duncan, Joshua C., Harrison, Luke D., Bartholomew, Calvin H., and Hecker, William C.. Effects of Particle Size and Shape on the Performance of a Trickle Fixed-Bed Recycle Reactor for Fischer-Tropsch Synthesis, *Ind. Eng. Chem. Res.*, 54, No 11), 2902-2909 (2015).
- Dormand, J. R., and Prince, P. J. A family of embedded Runge-Kutta formulae, *J. Comp. Appl. Math.*, 6, No 1), 19-26 (1980).
- Hou, B., Zhang, H., Li, H., and Zhu, Q. . Determination of the intrinsic kinetics of iron oxide reduced by carbon monoxide in an isothermal differential micro-packed bed, *Chinese. J. Chem. Eng.*, 23, No 6), 974-980 (2015).
- Jozwiak, W. K., Kaczmarek, E., Maniecki, T. P., Ignaczak, W., and Maniukiewicz, W. Reduction behavior of iron oxides in hydrogen and carbon monoxide atmospheres, *Appl. Catal. A-Gen.*, 326, No 1, 17-27 (2007).
- Kim, Y., and Worrell, E. International comparison of CO₂ emission trends in the iron and steel industry, *Energ. Policy.*, 30, No 10), 827-838 (2002).
- MIDREX, R&D. (2014). 2014 world direct production statistics.
- Monazam, E. R., Breault, R. W., and Siriwardane, R. Reduction of hematite (Fe₂O₃) to wüstite (FeO) by carbon monoxide (CO) for chemical looping combustion, *Chem. Eng. J.*, 242, No 1, 204-210 (2014).
- Negri, E.D., Alfano, O.M., and Chiovetta, M.G. . Direct reduction of hematite in a moving-bed reactor. Analysis of the water gas shift reaction effects on the reactor behavior, *Ind. Eng. Chem. Res.*, 30, No 3, 474-482 (1991).
- Nouri, S. M. M., Ale Ebrahim, H., and Jamshidi, E. Simulation of direct reduction reactor by the grain model, *Chem. Eng. J.*, 166, No 2, 704-709 (2011).
- Parisi, D. R., and Laborde, M. A. Modeling of counter current moving bed gas-solid reactor used in direct reduction of iron ore, *Chem. Eng. J.*, 104, No 1-3, 35-43 (2004).
- Pineau, A., Kanari, N., and Gaballah, I. Kinetics of reduction of iron oxides by H₂: Part I: Low temperature reduction of hematite, *Thermochim. Acta.*, 447, No 1), 89-100 (2006).
- Szekely, J, and El-Tawil, Y. The reduction of hematite pellets with carbon monoxide-hydrogen mixtures, *Metall. Mater. Trans. B.*, 7, No 3), 490-492 (1976)..
- Szekely, J., Evans, J.W., and Sohn, H.Y. *Gas-solid reactions* (Vol. 66). Academic Press New York, (1976)
- Takenaka, Y., Kimura, Y., Narita, K., and Kaneko, D. Mathematical model of direct reduction shaft furnace and its application to actual operations of a model plant, *Comput. Chem. Eng.*, 10, No 1), 67-75 (1986)..
- Tsay, Q. T., Ray, W. H., and Szekely, J. The modeling of hematite reduction with hydrogen plus carbon monoxide mixtures: Part I. The behavior of single pellets, *AIChE J.*, 22, No 6, 1064-1072 (1976).
- Tsay, Q.T., Ray, W. H, and Szekely, J. The modeling of hematite reduction with hydrogen plus carbon monoxide mixtures: Part II. The direct reduction process in a shaft furnace arrangement, *AIChE. J.*, 22, No 6), 1072-1079 (1976).
- Valipour, M. S., Motamed Hashemi, M. Y., and Saboohi, Y. . Mathematical modeling of the reaction in an iron ore pellet using a mixture of hydrogen, water vapor, carbon monoxide and carbon dioxide: an isothermal study, *Adv. Powder. Technol.*, 17, No 3), 277-295 (2006).
- Valipour, M. S., and Saboohi, Y. . Modeling of multiple noncatalytic gas-solid reactions in a moving bed of porous pellets based on finite volume method, *Heat. Mass. Transfer.*, 43, No 9), 881-894 (2007).

